

Impact of strong disorder on the static magnetic properties of the spin-chain compound $\text{BaCu}_2\text{SiGeO}_7$

done for homogeneous systems.¹⁴ Starting from the distribution of unrenormalized exchange couplings $P(J_i, J)$, where J is the energy cutoff, an effective low-energy theory is constructed by tracking, via flow equations, the behavior of $P(J_i, J)$ as the cutoff $J \sim k_B T$ is progressively reduced. In the RSS theory, the flow of the distribution of unrenormalized bond energies $P(J_i)$ depends on the considered energy scale and temperature.^{2,3} As a result, the static magnetic properties are dominated by a temperature-dependent population of effectively paramagnetic moments $n(T)$. Their characteristic energy- (ω) and temperature-dependent average spatial separation $\xi(T, \omega = 0) \sim n^{-1}(T) = \log^2(J_0/k_B T)$ diverges as $T \rightarrow 0$, leading to a quasi long-range ordered ground state.³ In the expression for $n^{-1}(T)$, J_0 is the largest exchange coupling in the chain prior to the renormalization.¹⁵ Due to weak residual interchain interactions, a magnetic order at a Néel temperature $T_N > 0$ K is established also in the random Heisenberg chains, albeit with a lower ordering temperature in comparison with the disorder-free case.^{16,17} In the present work we focus our attention on the local and bulk static magnetic properties of $\text{BaCu}_2\text{SiGeO}_7$ for $T > T_N$ and $H \neq 0$.

II. $\text{BaCu}_2\text{SiGeO}_7$: SUMMARY OF PREVIOUS RESEARCH

The experimental work on $\text{BaCu}_2\text{SiGeO}_7$ began with studies on tunable super-exchange interactions in spin-chain systems by Yamada *et al.* [12]. Across the series from $\text{BaCu}_2\text{Si}_2\text{O}_7$ to $\text{BaCu}_2\text{Ge}_2\text{O}_7$ the $\text{BaCu}_2(\text{Si}_{1-x}\text{Ge}_x)_2\text{O}_7$ compounds ($0 < x < 1$) crystallize with a $Pnma$ space group. For $x = 0.5$, corresponding to maximum disorder in the exchange couplings, the values of the lattice parameters are $a = 6.917(7)$ Å, $b = 13.28$ Å, and $c = 6.944(7)$ Å,¹⁸ in between the parameters of the two end members of the series. The spin chains run along the crystallographic c axis, as shown in Fig. 1.

Early magnetization measurements of polycrystalline samples revealed the often observed broad maximum of $\chi(T)$, also known as the Bonner-Fisher peak.¹⁹ This maximum shifts linearly with x towards higher temperatures as the Ge concentration is enhanced. From this feature it was initially deduced that the high-temperature properties of $\text{BaCu}_2\text{SiGeO}_7$ effectively reflect those of a standard spin-1/2 Heisenberg chain with $J_{\text{eff}} = (J_{\text{Si}} + J_{\text{Ge}})/2 \approx 37$ meV, where $J_{\text{Si}} = 24.1$ meV and $J_{\text{Ge}} = 50$ meV represent the intrachain exchange interactions for no and for complete Ge substitution, respectively. The enhancement of the AFM exchange, resulting from a higher Ge content, was explained in terms of a change of the Cu-O-Cu bonding angle, from $\phi = 124^\circ$ in $\text{BaCu}_2\text{Si}_2\text{O}_7$ to 135° in the Ge parent compound.²⁰

Earlier bulk measurements already revealed two distinct features:¹² (i) a low-temperature divergence of the spin susceptibility in $\text{BaCu}_2\text{SiGeO}_7$, interpreted as a simple Curie-type behavior due to uncompensated magnetic

moments,²¹ and (ii) a low-temperature magnetic order, expected even in the case of random Heisenberg chains (RHCs),¹⁷ with an onset at $T_N = 0.7$ K in $\text{BaCu}_2\text{SiGeO}_7$.¹⁸

In zero magnetic field, $\text{BaCu}_2\text{Si}_2\text{O}_7$ is known to order antiferromagnetically at $T_N = 9.2$ K.²² The more than tenfold reduction of T_N in $\text{BaCu}_2\text{SiGeO}_7$, may be related to the fact that the introduction of Ge modifies not only the intrachain, but also the interchain coupling which, along the a -axis, changes from FM- to AFM-type.¹² The latter implies that for $\text{BaCu}_2\text{SiGeO}_7$ the interchain coupling alternates in sign and, therefore, it averages out to a mean-field value.²³

The interest in $\text{BaCu}_2\text{SiGeO}_7$ grew significantly as soon as results of magnetic-susceptibility measurements on single crystals appeared in the literature.²¹ They suggested a logarithmic dependence of the low-temperature spin susceptibility,²¹ consistent with predictions of the RHC model.² Subsequent inelastic neutron-scattering (INS) studies focused on the measurement of the energy dependence of the correlation length $\xi(T = 0, \omega)$, which at zero-temperature is inversely proportional to the free-spin concentration $\xi(\hbar\omega) \sim n^{-1}(\hbar\omega) = \log^2(J_0/\hbar\omega)$, with $\hbar\omega$ the energy of the probing neutrons. In INS, ξ is extracted from the inverse width of the energy-integrated scattering intensity $S(\mathbf{q})$ which, in case of a disordered phase, is typically of Lorentzian shape.²⁴ Following some earlier misinterpretation of the data due to problems with background subtraction,^{21,25} the INS results were found to be quantitatively consistent with a Luttinger-liquid behavior reflecting a disorder-free spin chain with a single effective coupling $J_{\text{eff}} \approx 37$ meV.¹⁸ It was concluded that the expected RHC-related physics must manifest itself at energies much lower than those accessible by neutron experiments. In a previous NMR study¹⁵ we already pointed out how the spin dynamics of $\text{BaCu}_2\text{SiGeO}_7$, probed at the characteristic Larmor energy $\hbar\omega_L \sim 1$ μeV (with $\omega_L/2\pi$ the NMR resonance frequency), turns out to be notably different with respect to that of the regular Heisenberg chain $\text{BaCu}_2\text{Si}_2\text{O}_7$. On the other hand, considering existing data on $\text{BaCu}_2\text{Si}_2\text{O}_7$ and $\text{BaCu}_2\text{Ge}_2\text{O}_7$, a low-temperature divergence of the magnetic susceptibility also in $\text{BaCu}_2\text{SiGeO}_7$ is not really surprising.¹³ In addition, since INS failed to detect any sort of disorder-induced spin dynamics in this compound, the existence of a random-singlet state (RSS — the ground state of the isotropic RHC Hamiltonian) was considered questionable. In the present work we show how the effect of disorder on the *static* magnetic properties can be quantitatively modeled and compared with experiments, thereby supporting the RHC scenario.

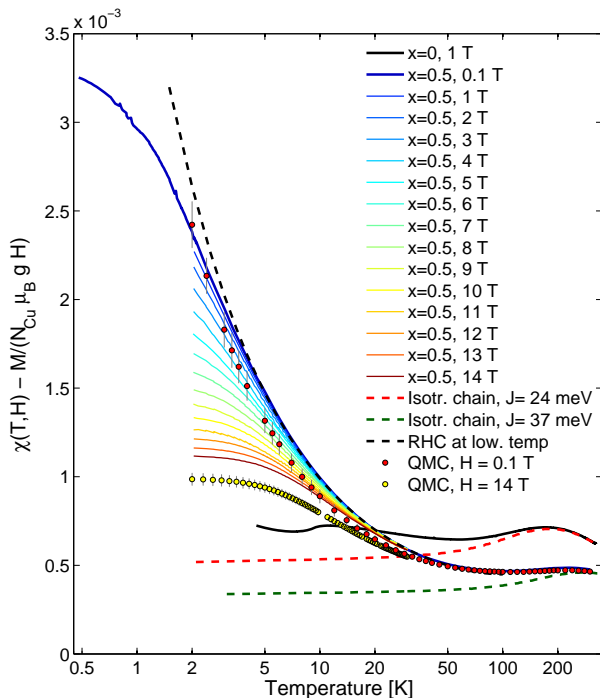


FIG. 2. (color online) Field and temperature dependences of the magnetic susceptibility $\chi(T, H)$ per Cu ion in $\text{BaCu}_2\text{SiGeO}_7$ (and in $\text{BaCu}_2\text{Si}_2\text{O}_7$, at 1 T) with $\mathbf{H} \parallel b$ in normalized units, assuming $g = 2$.¹³ The fit of $\chi(T, 0.1 \text{ T})$ with an RHC model was adopted from Ref. 3, while the $\chi(T)$ curves for chains with a single isotropic exchange value were calculated as in Ref. 26. QMC simulations of the $\chi(T, H)$ susceptibility at $\mu_0 H = 0.1$ and 14 T for a simple J_1 - J_2 RHC model is also shown (see text for details).

III. MAGNETIC SUSCEPTIBILITY OF $\text{BaCu}_2\text{SiGeO}_7$

A. Experimental results

As a first step, we extended the measurements of the magnetic susceptibility $\chi(T, H)$ to wider temperature and field ranges than those covered in previous studies. Single crystals of $\text{BaCu}_2\text{SiGeO}_7$ were grown by the floating-zone technique. One of them was cut and the smaller 6.5-mg part was used in magnetometry measurements; the remaining 20-mg piece was used for the NMR investigations.

The magnetization of the chosen sample was measured by applying a magnetic field $\mathbf{H} \parallel b$. Magnetic susceptibility data $\chi = M/H$ are displayed as bold solid lines in Fig. 2. For $\mu_0 H = 0.1 \text{ T}$ and at temperatures $T \geq 1.8 \text{ K}$, the measurements were performed using a standard dc SQUID magnetometer, whereas to cover temperatures down to 0.5 K we employed a SQUID device with a ^3He insert. For all the other fields and for temperatures $T \geq 1.8 \text{ K}$ we used a vibrating-sample magnetometer (VSM). Since in the latter case data are collected “on the fly”, i.e., while the temperature is being

swept at 0.25 K/min, this causes a small (known) temperature difference between sample and thermometer position. In addition, a certain dispersion in the magnetization values was reduced by applying a moving-average filter with a 200-mK width to the raw experimental data. Magnetic hysteresis, defined as the difference between the zero-field-cooled and field-cooled magnetization data, was observed for $T < 800 \text{ mK}$. The hysteretic behavior is probably related to ferromagnetic domains with a rather small net magnetic moment present in the ordered low-temperature phase. Since only the zero-field-cooled scans are relevant for our discussion, the field-cooled data are not shown.

B. Data analysis

As shown in Fig. 2, for temperatures above 30 K the $\chi(T, H)$ curves are field-independent and, for $T > 200 \text{ K}$, they approach the theoretical prediction for an *isotropic* Heisenberg chain²⁶ with an exchange parameter $J_{\text{eff}} = (J_{\text{Si}} + J_{\text{Ge}})/2 \approx 37 \text{ meV}$ (see the green dashed line in Fig. 2). For comparison, the red dashed line indicates the calculated $\chi(T)$ for an isotropic chain with $J_{\text{Si}} \approx 24 \text{ meV}$, corresponding to the $x = 0$ case.

We first discuss two major differences between the magnetic susceptibilities of $\text{BaCu}_2\text{Si}_2\text{O}_7$ ($x = 0$) and $\text{BaCu}_2\text{SiGeO}_7$ ($x = 0.5$): (i) Our previous successful attempt to interpret the low-temperature increase/divergence of $\chi(T)$ in $\text{BaCu}_2\text{Si}_2\text{O}_7$ and $\text{BaCu}_2\text{Ge}_2\text{O}_7$ as simply being caused by a local transverse staggered field (LTSF,¹³ see Sec. IV B) is inadequate for treating the more complex case of $\text{BaCu}_2\text{SiGeO}_7$. First of all, the magnetic susceptibility $\chi(T < 10 \text{ K}, H)$ is strongly *reduced* even by moderate fields. As a result, the magnetization deviates from the linear response with respect to H (see Fig. 7 and Ref. 26), expected either for an isotropic chain in the LL regime, or for the sine-Gordon (SG) model in the high-temperature limit, the latter describing the physics when an LTSF is present.¹³

The SG model, even at intermediate temperatures, is inadequate to describe the physics of $\text{BaCu}_2\text{SiGeO}_7$. Indeed, in this case $\chi(T)$ is known to exhibit a symmetric peak centered at a temperature T_m , roughly corresponding to half of the field-induced gap Δ_{SG} .²⁷ To exemplify this fact, we consider the Hamiltonian in Eq. (1) with $J_i = J$ and $H \neq 0$. In the reduced units $h_{i,\perp}^* = \mu_B H_{i,\perp} / J_{\text{eff}}$, with $H_{i,\perp} = (-1)^i c H$, this model features a gap Δ_{SG} in the spin-excitation spectrum which, for $h_{\perp}^* \ll 1$, scales as:²⁸

$$\frac{\Delta_{\text{SG}}}{J} = 1.78 \cdot (h_{\perp}^*)^{\frac{2}{3}} \cdot (-\log h_{\perp}^*)^{1/6}. \quad (2)$$

Equation (2) implies that for $c = 0.092$ (the value estimated for $\text{BaCu}_2\text{Si}_2\text{O}_7$ ¹³ if $\mathbf{H} \parallel b$), the LTSF yields $\Delta_{\text{SG}} \simeq 1.42 \text{ meV}$ at $H = 14 \text{ T}$, corresponding to $T_m \simeq 8.2 \text{ K}$. On the other hand, as can be seen in Fig. 2,

the susceptibility recorded at 14 T tends to saturate at low temperatures, rather than display a peak at T_m .

(ii) The inadequacy of the SG model in interpreting the $\chi(T, H)$ data of $\text{BaCu}_2\text{SiGeO}_7$ is particularly evident from the (T, H) -dependence of T_i , the inflection point which marks the start of saturation (corresponding to the maximum of $|\partial M/\partial T|$ in a fixed field H — see Fig. 3). To overcome noise problems in the calculation of $|\partial M/\partial T|$ from raw magnetization data, the experimental points were linearly interpolated using a 200-mK binning and the resulting line slope was taken as the derivative with respect to temperature. The results of this procedure are shown as colored circles in Fig. 3 for four selected fields. A (T, H) color map of the $|\partial M/\partial T|$ values is shown in Fig. 4a. Here the inflection points (assigned with an error corresponding to the peak width at 95% of the peak height in Fig. 3) are shown as open circles. The resulting $T_i(H)$ values follow a linear field dependence, such that $k_B T_i = 0.744(7) \mu_B H$. Besides requiring a nonuniversal dimensionless prefactor,²⁹ the field dependence of T_i does not follow the $H^{2/3}$ power law that the small $h_{i,\perp}^*$ value would imply for $\Delta(H)/2$.²⁷ The calculated dependences of $\Delta/2$ for $H_\perp = (-1)^i c H$ with $c = 0.092$ or 0.052 are both also shown in Fig. 4a. The first c value represents the LTSF proportionality constant in $\text{BaCu}_2\text{Si}_2\text{O}_7$.¹³ Because of the similar local environments, it seems reasonable to use the same value also for $\text{BaCu}_2\text{SiGeO}_7$. The reason for choosing $c = 0.052$ instead, will be clarified in Sec. IV.

In view of these two inadequacies, we modified our previous approach to the experimental data analysis¹³

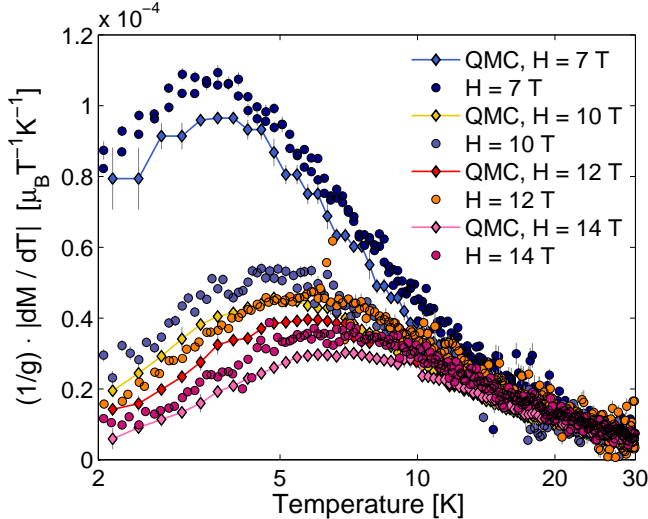


FIG. 3. (color online) First derivative of the sample magnetization vs. temperature, $|\partial M(T, H)/\partial T|$, in $\text{BaCu}_2\text{SiGeO}_7$ for $H \parallel b$. The graphic compares several cross sections of the color map shown in Fig. 4. The assigned errors reflect the line-slope uncertainty for fits within the binning range (see text for details). The shown QMC simulation results were obtained *without* using any free parameters.

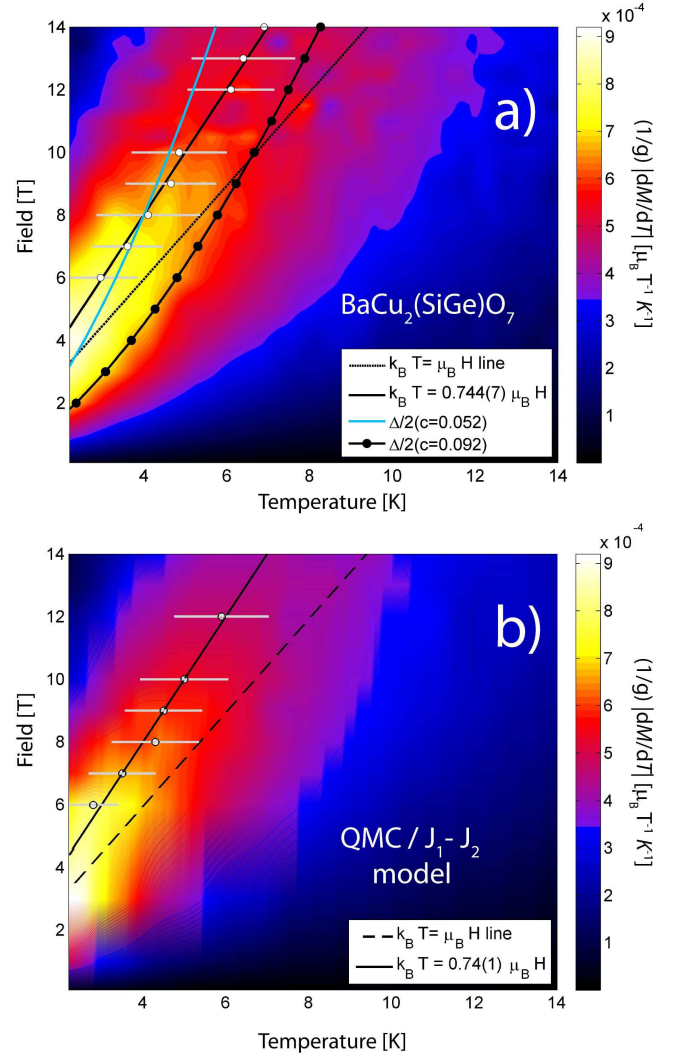


FIG. 4. (color online) (a) First derivative of the sample magnetization vs. temperature, $|\partial M(T, H)/\partial T|$, in $\text{BaCu}_2\text{SiGeO}_7$ for $H \parallel b$ (data scaled using $g = 2$).¹³ The open circles represent cross-over temperatures. For details on data treatment and for a description of the plotted lines see text. (b) QMC simulation of the J_1 - J_2 RHC model for a system of 6000 spins, using 20 realizations of disorder for each (T, H) -point. The color map was generated using the same data treatment as in panel (a).

and instead chose to compare the experimental results with the predictions of the RHC model Hamiltonian in Eq. (1).³ A first comparison is carried out by fixing $c = 0$ and by assuming the J_i values to be uniformly distributed between the two limits, J_{Si} and J_{Ge} .

In case of nonzero temperatures and magnetic fields, the renormalization flow of the decimation procedure is interrupted either at the thermal energy $k_B T$, or at the magnetic energy $g \mu_B \langle S \rangle H$.²⁹ In the first case, the resulting susceptibility is:³

$$\chi(T)_{\text{RHC}} \sim T^{-1} \log^{-2}(J_0/k_B T). \quad (3)$$

In the second case, the system is driven away from the zero-field fixed point into a regime with field-aligned undecimated spins, a saturated magnetization and zero entropy.²⁹ In spin-1/2 AFM-RHCs the decimation procedure involving the total set of spins leaves the renormalized magnetization magnitude at $\langle S \rangle = 1/2$, unlike, for example, in an RHC with FM-AFM coupling.²⁹ For this reason, the onset of saturation of the low-temperature magnetization occurs at $k_B T_i \approx \mu_B H$.²⁹ A fit to the susceptibility data at the smallest applied field, using the theoretical random-singlet expression for $\chi(T)_{\text{RHC}}$, is shown in Fig. 2 as a black dashed line. A rather good match is found above 4 K with a cutoff $J_0 \simeq 66.3 \pm 0.7$ meV.

To achieve a more quantitative comparison, we carried out a series of Quantum Monte Carlo (QMC) simulations based on Eq. (1), where J_i couplings alternate randomly from $J_1 = J_{\text{Si}} = 24.1$ meV to $J_2 = J_{\text{Ge}} = 50$ meV (we call this a J_1 - J_2 model), mimicking the situation expected for $\text{BaCu}_2\text{SiGeO}_7$. We chose 6000 spin sites with randomly distributed but equally probable J_1 and J_2 couplings. The simulations for $\chi(T, H)$ were averaged over at least 25 random realizations of disorder, as obtained from a directed-loop algorithm³⁰ within the ALPS 2.0 package.¹¹ Technical details related to the QMC simulations are discussed in App. A. Disorder in the exchange couplings was imposed by assuming an equal number ($L/2$, with L as the chain length) of J_1 and J_2 values, randomly permuted to construct the RHC chain that was to be simulated.

Selected results of these simulations are shown as red and yellow circles in Fig. 2, as interconnected diamonds in Fig. 3, and as a color map in Fig. 4b. In view of the simplicity of the model, the qualitative and quantitative agreement of our parameter-free QMC simulations with the data is remarkable. Incidentally, the best fit of the RS prediction to the low- T QMC results in an applied field $\mu_0 H = 0.1$ T requires $J_0 \approx J_2$. This corresponds to the largest energy scale in the system before the decimation starts, thus reinforcing the pertinence of the theory used to capture the magnetic properties of the system. As may be seen in Figs. 3 and 4b, by applying the moving-average procedure described above also to the QMC results, numerical calculations predict the same free-spin-like linear field-dependence for T_i as observed experimentally. This is an important result, because the existence of paramagnetic entities at $T = 10$ K in a strongly-correlated system, with a characteristic energy scale corresponding to a temperature exceeding 200 K, is highly counterintuitive.

IV. NUCLEAR MAGNETIC RESONANCE IN A RANDOM HEISENBERG CHAIN

Although the measurements of $\chi(T, H)$ and the comparison with QMC calculations already provide a strong indication for the formation of an RS phase in $\text{BaCu}_2\text{SiGeO}_7$ at low temperatures, it is tempting to directly

verify the presence of a random-singlet state on a local scale. With decreasing temperature an increasing number of spins form pairs by adopting a nonmagnetic singlet ground state. The divergent low-temperature tail of $\chi(T, H)$ is due to the residual unpaired spins. The tendency to form a random-singlet ground state should be directly manifest in NMR data, reflecting a growing number of ^{29}Si sites which experience a zero net transferred local field.

A. Experimental results

Height-normalized ^{29}Si NMR lines, as recorded in a 7-T external field applied along the crystallographic b axis, are plotted in Fig. 5. The spectra were obtained by superposing several acquisitions in the frequency-sweep mode, as described in Ref. 31.

The effects of disorder are evident already by comparing the high-temperature line shapes of $\text{BaCu}_2\text{SiGeO}_7$ and $\text{BaCu}_2\text{Si}_2\text{O}_7$ (see inset of Fig. 5). We note that the ^{29}Si resonance of $\text{BaCu}_2\text{SiGeO}_7$, apart from being broader than that of its pristine counterpart, is also shifted to higher frequencies. We recall that NMR data of $\text{BaCu}_2\text{Si}_2\text{O}_7$ (taken at $\mu_0 H = 7$ T, with $\mathbf{H} \parallel b$) exhibit a positive orbital shift of $\sigma_b \simeq 0.018$ MHz, with a *negative* hyperfine-coupling to the longitudinal magnetization.¹³ As shown in Fig. 2, the high-temperature magnetization of $\text{BaCu}_2\text{SiGeO}_7$ is equivalent to that of an isotropic chain with $J = 37$ meV and is distinctly smaller than that of $\text{BaCu}_2\text{Si}_2\text{O}_7$, well modelled by choosing $J = 24.1$ meV. Consequently, the negative hyperfine shift in case of a sample with disorder is smaller and, hence, the resonance is located closer to σ_b (see inset of Fig. 5). This result is ultimately an independent confirmation of the validity of the model which allowed us to extract the parameter σ_b in Ref. 13. We emphasize that, due to a random variation of the hyperfine interactions, a broadening of the resonance in the $x = 0.5$ case may well be of structural origin, rather than due to magnetic disorder. Realistically, both structural and magnetic disorder have to be taken into account and one of the aims of the analysis outlined below is to disentangle them. Another striking feature of the NMR signals is the temperature-dependent shift of the line maxima. In Fig. 5 this shift is evidenced by comparing the sequence of yellow points, marking the maxima, with the vertical dashed line, representing the peak position of the 300-K line. It indicates a growing nonzero uniform magnetization as the temperature is lowered, in obvious contradiction to the RS-phase hypothesis, where the formation of singlets would imply the absence of a local magnetization. As expected, unlike to what is observed in $\text{BaCu}_2\text{Si}_2\text{O}_7$,^{13,22} the NMR data show no indications of a phase transition around $T = 10$ K for the disordered compound.

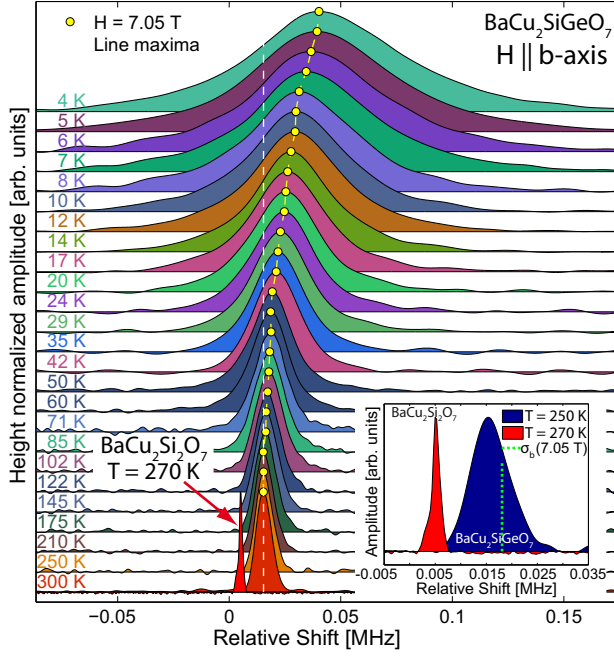


FIG. 5. (color online) Temperature dependence of the ^{29}Si NMR lines of the disordered Heisenberg chain compound $\text{BaCu}_2\text{SiGeO}_7$ in a magnetic field of 7.05 T applied along the b -axis. The zero frequency marks the resonance of ^{29}Si nuclear spins in a standard reference sample such as $\text{Si}(\text{CH}_3)_4$.³² The white dashed line marks the position of the resonance at room temperature, while the yellow points represent the position of the maxima, displaying a shift towards higher frequencies at low temperatures. The inset compares the cases of maximum and no disorder at high temperature. The green dashed line marks the orbital shift as obtained from Ref. 13 (see text for details).

B. Data analysis

In order to interpret the recorded NMR line shapes and positions, we compare the experimental data with the results of QMC simulations of the J_1 – J_2 model, addressed in Sec. III. In Fig. 6a we show the temperature-dependent, height-normalized histograms, which reflect the occurrences of longitudinal local magnetization values S_i^z in $10^{-3} \mu_B$ intervals for $\mu_0 H = 7$ T (z is the spin quantization axis along which the external field was applied). The histograms were obtained by using a single configuration of disorder in a system of $L = 6000$ spins. We note that at $T = 300$ K the S_i^z values are distributed around a nonzero, albeit small, uniform magnetization. In this regime the details of disorder are not essential for describing the physics. At low temperatures, however, a broadened magnetization peak appears, centered at zero local moment, as expected in the case of a continuous formation of singlets. At the same time we observe weak but extremely broad tails (see top histogram in Fig. 6a), indicating the presence of incompletely compensated spins, which are progressively polarized as the temperature is reduced.

As shown in Fig. 6b, the local-moment distribution obtained from these simulations (which do not include an LTSF) does not match the experimental NMR data. The formation of random singlets implies that at a significant number of sites the moments of the Cu atoms are quenched at low temperatures, corresponding to a zero shift of the simulated NMR line, in disagreement with observations. It turns out that it is essential to consider the combined effect of random exchange interactions and an LTSF, namely to set $c \neq 0$ in the Hamiltonian (1). To include an LTSF we use the same approximation made in the case of no disorder,^{13,27} i.e., we assume the total local magnetization \mathbf{m}_i to be the sum of a non-uniform longitudinal and a transverse contribution, in the form:

$$\mathbf{m}_i = \langle \mathbf{S}_i^\parallel \rangle + \langle \mathbf{S}_i^\perp \rangle, \quad (4)$$

where for the magnitude of the local transverse magnetization we write $\langle S_i^\perp \rangle(H, H_{i,\perp}) \approx \langle S_i^\perp \rangle(0, H_{i,\perp})$, and analogously for the longitudinal component, with $H_{i,\perp} = c_i H$.¹³ Because of this particular approximation, two QMC simulations, one for S_i^\perp and another for S_i^\parallel , can be carried out separately on a diagonal basis.

With $H \neq 0$, an LTSF acts on paired spins by mixing the nonmagnetic singlet states $|s\rangle$ with the magnetic triplet states $|t_{+1}\rangle = |\uparrow_1\uparrow_2\rangle$ and $|t_{-1}\rangle = |\downarrow_1\downarrow_2\rangle$, thereby inducing a nonzero magnetization also in the ground state of the spin pair.³³ If both the uniform field and the LTSF are considered, in a first-order perturbation approximation, the new ground state can be written as:³³

$$|s'\rangle \approx |s\rangle + \alpha_+ |t_{+1}\rangle - \alpha_- |t_{-1}\rangle, \quad \text{where} \\ \alpha_\pm \propto \frac{cH\mu_B}{J \mp g\mu_B H}.$$

The uniform field appearing in the denominator can be neglected if $J \gg g\mu_B H$, which is the case for the strongest coupled singlets in the RS phase. Therefore, at temperatures $k_B T \approx \min(J) \gg g\mu_B H$ the longitudinal local magnetization varies linearly with the applied field. Here $\min(J)$ refers to the minimum exchange coupling value of the already formed singlets.

The distribution of local-magnetization values in a J_1 – J_2 RHC model which includes an LTSF is shown in Fig. 6c. Clearly, the presence of an LTSF substantially modifies the magnetization profiles shown in Fig. 6a. By assuming that the local symmetry of the oxygen atoms surrounding a Cu^{2+} ion is largely unaffected by the Si-to-Ge substitution, the same value of $c = 0.092$ obtained for $\text{BaCu}_2\text{Si}_2\text{O}_7$ ought to be valid also in our case. As seen in Fig. 6c, at $T = 300$ K and $\mu_0 H = 7$ T, the chosen LTSF is too weak to induce a nonzero magnetization. However, as the temperature is progressively lowered, singlets with a *distribution* of effective exchange couplings are formed and a staggered field $H_{i,\perp}$ acting on them creates a distributed local magnetization of the form $\langle S_i^\perp \rangle \propto \mu_B H_{i,\perp} / J_i$. Therefore, the histograms in Fig. 6c split and broaden with decreasing temperature. The symmetrical splitting reflects the alternating sign of

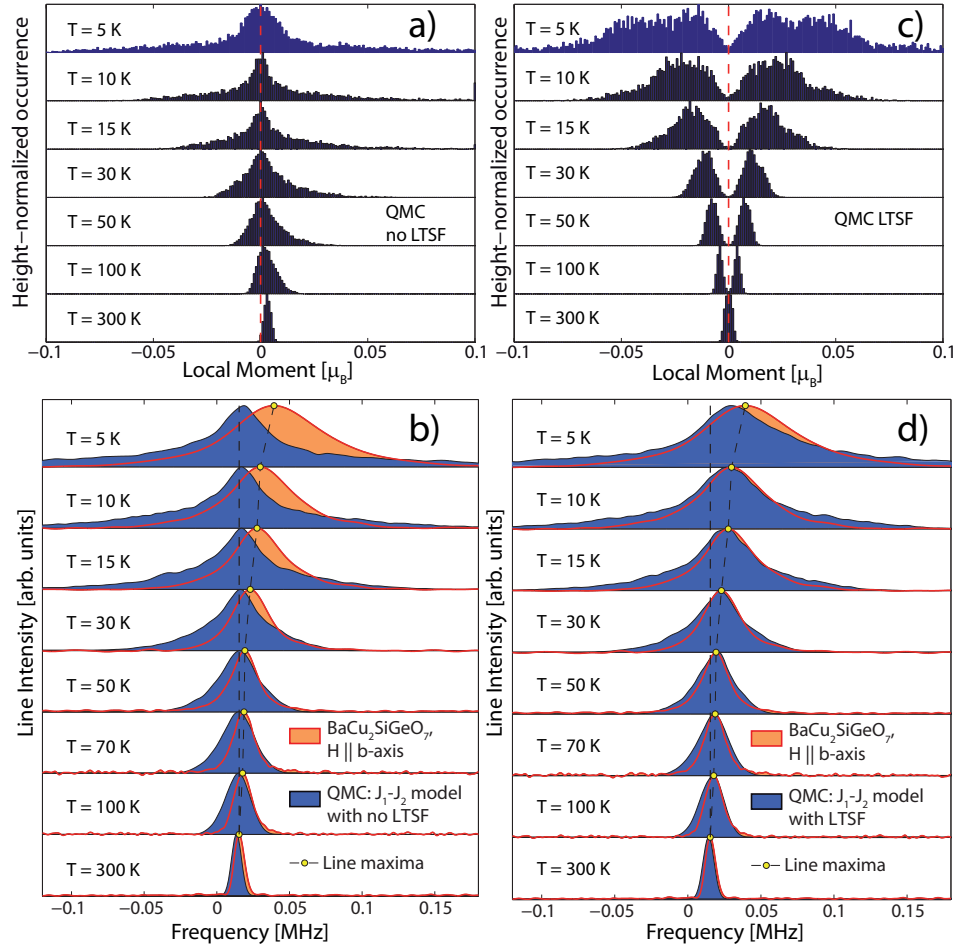


FIG. 6. (color online) (a) QMC simulation of the local magnetization of a J_1 - J_2 model of a spin-chain with 6000 sites placed in an external field of 7 T. The number of occurrences of the magnitude of a certain local moment is plotted, with each occurrence calculated in equidistant intervals of $10^{-3}\mu_B$ and normalized to the most frequent one. The red dashed line marks the zero. (b) Simulated NMR line shapes (blue) using the results obtained from (a) and compared with the experimental data (orange). The black dashed line at fixed frequency marks the position of the peak of the $\text{BaCu}_2\text{SiGeO}_7$ line at 300 K. No LTSF is present in this case. (c) Same as in (a), but with the uniform field replaced by a staggered field $H_{i,\perp} = (-1)^i cH$, with $c = 0.092$ and $\mu_0 H = 7$ T. (d) Same as in (b), but including an LTSF in the model (see text for details).

the LTSF from site to site, with a mean absolute value of the local moment which progressively shifts away from $|\langle S_i^\perp \rangle| = 0$.

In order to compare the simulated local magnetization profiles with the NMR line shapes, structural details have to be considered. Eight configurations of disorder in systems with $L = 6000$ sites were simulated. In order to reproduce 6000 unit cells, the local moments were then arranged into four different chains, with two inequivalent copper atoms each. At this first stage, the dipolar coupling was neglected, but we considered the hyperfine coupling to both the longitudinal and the transverse magnetization. Following the notation of Ref. 13, for $\mathbf{H} \parallel b$, the local hyperfine field h_{loc} at a general ^{29}Si nuclear site can be written as:

$$h_{\text{loc}} = \sum_{i=1}^4 \left(a_i \langle S_i^\parallel \rangle + b_i \langle S_i^\perp \rangle \right), \quad (5)$$

where the index i runs over the four nearest-neighbor copper sites. With this notation, the relative NMR resonance frequency $^{29}\omega$ can be written as $^{29}\omega \approx \gamma h_{\text{loc}} + \sigma_b$, with γ as the ^{29}Si nuclear gyromagnetic ratio. From our previous study¹³ of $\text{BaCu}_2\text{Si}_2\text{O}_7$ we can fix the parameters $\sum_i a_i \simeq -0.16$ T/ μ_B , $\sum_i (-1)^i b_i \simeq 0.128$ T/ μ_B , whereas $\sigma_b \simeq 0.018$ MHz at 7 T. Each of the above hyperfine parameters, which couple the silicon nuclear magnetism to the longitudinal and transverse electronic magnetization of copper, represents the sum of four individual copper-to-silicon couplings. Given the broken translational symmetry due to disorder, the individual Cu-Si couplings are essential for a quantitative comparison between data and theory. Unfortunately, these cannot be evaluated by experiment, leaving six unknown free parameters in the model.

For a comparison of the simulated NMR lines with data recorded at 5 K, we used the following parameters (in

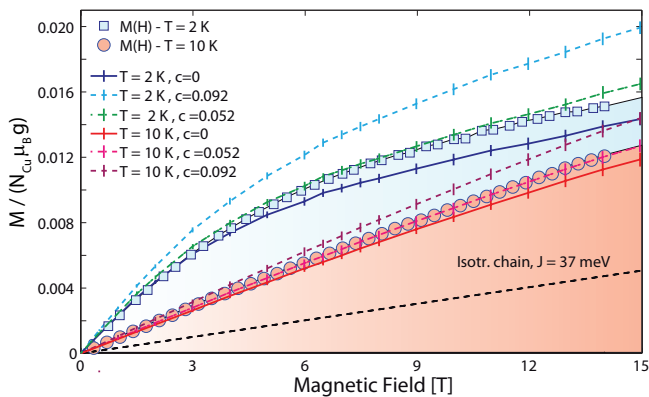


FIG. 7. (color online) Field dependence of the magnetization of $\text{BaCu}_2\text{SiGeO}_7$ at 2 and 10 K (dots) and comparison with QMC simulations of the $J_1 - J_2$ RHC model without ($c = 0$) and with ($c \neq 0$) LTSF. The c coefficient refers to the staggered field value $H_{i,\perp} = (-1)^i cH$, with H the uniform field. Also shown is the field dependence of the ground state magnetization ($T = 0$ K) of an isotropic Heisenberg spin- $1/2$ chain, as from Ref. 26. The magnetization is expressed in normalized units (N is the total number of copper sites and μ_B is the Bohr magneton), assuming $g = 2$.

T/μ_B units): $b_1 = b_3 = -0.24$, $b_2 = -0.07$ for the coupling to the transverse magnetization, and $a_1 = -0.16$, $a_2 = 0.08$, $a_3 = -0.015$ for the coupling to the longitudinal one. The sign of the parameters b_i changes according to the considered Si nucleus. By making use of them and with no other free parameters, we succeeded in simulating the complete temperature dependence of the NMR lines, which account for the simultaneous presence of both an LTSF and a uniform magnetic field. The result is shown in Fig. 6d, where the agreement between data and the theoretical model is again remarkable.

To be more specific, for a comparison with the experiment, we calculated the line shapes by convoluting the distribution of local fields at the ^{29}Si sites with a 2-kHz wide Gaussian, which is equivalent to the width of the line profile of pure $\text{BaCu}_2\text{Si}_2\text{O}_7$, shown in the inset of Fig. 5. The choice of the optimal binning range, which strongly affects the shape of the tails of the S_i^z histograms in Fig. 6, was done by employing the algorithms proposed in Refs. 34 and 35. Note that the lines displayed in Fig. 6d show that the averaging process over four Cu sites removes the splitting in the original histograms in Fig. 6c. In addition, the simulated lines shift with temperature, as indeed observed in the experiment. The minimally-shifted line shape at $T = 300$ K reflects magnetic disorder. By comparing Figs. 6b and 6d, it may be seen that the inclusion of an LTSF in the simulations significantly improves the agreement between theory and experiment. Therefore, from both a macroscopic and a local point of view, NMR data confirm that the static magnetic properties of $\text{BaCu}_2\text{SiGeO}_7$ are those of an RHC, with the addition of a residual LTSF.

To cross check the consistency of the proposed model,

it seems natural to consider the LTSF-induced effects also in the magnetometry data. Since the influence of the LTSF grows with the applied field H , we consider the calculated $M(H)$ curves (shown by dotted lines in Fig. 7) at two representative temperatures, $T = 2$ K and 10 K. The calculation of $M(H)$ at $T = 2$ K, using the average exchange coupling $J = 37$ meV, reflects the *linear* behavior expected for an isotropic Heisenberg chain in its LL regime²⁶ and differs substantially from the experimental data. In fact, this oversimplified model completely neglects the field-induced alignment of the still uncompensated spins that, in a random Heisenberg chain, survive even at the lowest temperatures. On the other hand, QMC simulations using the $J_1 - J_2$ model discussed in Sec. III and in Ref. 15 show significant improvements over the simplified “average- J ” model (solid blue and red lines in Fig. 7 for $T = 2$ K and 10 K, respectively).

The next refinement was to include both a uniform and a staggered magnetization in the $J_1 - J_2$ model and combine them²⁷ to obtain:

$$M(H, T) = \sum_i \left[\langle S_i^{\parallel} \rangle(H, T) + (-1)^i c \langle S_i^{\perp} \rangle(H_{i,\perp}, T) \right], \quad (6)$$

with $\sum_i \langle S_i^{\parallel} \rangle(H, T)$ the RHC magnetization in a uniform field. As can be seen in Fig. 7, the QMC calculation for $M(H, T)$ with $c = 0.092$ unexpectedly fails to reproduce the data. A good agreement with the magnetization scans at both temperatures was, however, obtained using $c \simeq 0.052$. The discrepancy in the prefactor is most probably due to the fact that the current model neglects the effects of structural disorder in $\text{BaCu}_2\text{SiGeO}_7$. A more refined model taking into account such subtleties, by including a site-dependent c value, was not implemented in the present analysis. Nonetheless, the essence of RHC physics, which dominates the magnetic properties of the probed system, is born out by the combined investigation of bulk magnetometry, NMR measurements and QMC simulations. Taken together they strongly suggest that $\text{BaCu}_2\text{SiGeO}_7$ is an excellent realization of a random Heisenberg chain model, as originally claimed in Ref. 15, thus providing the ideal testing ground for analytic theories modeling a random-singlet ground state.

V. SUMMARY AND CONCLUSIONS

In conclusion, we considered the $\text{BaCu}_2\text{SiGeO}_7$ compound, where spin- $1/2$ Cu^{2+} ions interact via random exchange couplings, as a representative of RHC systems with bond disorder. We demonstrate that this spin-chain material has a ground state which is very well described on the basis of the RHC Hamiltonian in Eq. (1).

By using temperature- and magnetic field-dependent microscopic ^{29}Si NMR measurements, combined with macroscopic magnetic-susceptibility data and results of detailed numerical Quantum Monte Carlo simulations, we find a coherent description of the physical proper-

ties of the system, compatible with that of an RS phase. In particular, the considerable broadening of the NMR lines and the divergent magnetic response at low temperatures, combined with a nonlinear increase of the magnetization as a function of field at low T , all reflect the presence of unpaired spins with arbitrary small couplings even at temperatures close to zero.

Specific refinements in the simulations of J_1 - J_2 model have shown that the addition of a local transverse staggered field — LTSF (similar to that present in the parent compound $\text{BaCu}_2\text{Si}_2\text{O}_7$)¹³ — is essential also for reproducing the observed NMR line shifts.

Since the magnetization of a singlet in an LTSF is proportional to the local field, the detection of the field distribution by future ^{63}Cu NMR measurements may provide a direct way to explore the J distribution in an RHC. In addition, besides the existing stretched-exponential NMR relaxation data,¹⁵ the spectral properties of random Heisenberg chains would be more directly accessible if neutron scattering experiments in a lower energy range would be possible.

ACKNOWLEDGMENTS

The authors thank A. Feiguin (Northwestern University, Boston), K. Prša (EPFL, Lausanne), and O. Zaharko (PSI, Villigen) for useful discussions. The $\text{BaCu}_2\text{SiGeO}_7$ samples used in this work were prepared in the early 2000's in the group of Prof. K. Uchinokura at the University of Tokyo. This work was financially supported in part by the Schweizerische Nationalfonds zur Förderung der Wissenschaftlichen Forschung (SNF) and the NCCR research pool MaNEP of SNF.

Appendix A: Error evaluation in the QMC simulations

In order to correctly interpret the numerical results, it is necessary to mention the theoretical expectations for the error bars in QMC simulations (i.e., specific to this method), in relation to the self-averaging induced errors (i.e., specific to disorder).³⁶ For a spin chain of length L , one can define the ratio $R_X(L) = (\overline{X^2} - \overline{X}^2)/\overline{X}^2$, where X is any macroscopic variable subject to self-averaging and \overline{X} denotes the same quantity averaged over the realizations of disorder.³⁶ By using 10^4 “Monte Carlo updates” (the number of random updates of the system performed by the algorithm before a new configuration is generated) and 10^5 independent Monte Carlo measurements in a system of 6000 spins, the relative error for $M(T, H)$ in low-temperature QMC simulations was found to be 10 times lower than $\sqrt{R_X(L)}$, the error due to the average on all the realizations of disorder. Therefore, in our case $\sqrt{R_X(L)}$ is the dominant simulation error. Whenever the correlation length is $\xi \sim \log^2(J_0/T) \ll L$, self-averaging can be justified based on the central-limit theorem.³⁶ In case of critical systems, where the correlation length tends to diverge ($\xi \gg L$), the only way to obtain meaningful results in the presence of disorder consists in increasing the system size L . By simulating systems with different spin-chain lengths L , we find that $\sqrt{R_X(L \rightarrow \infty)} = \sigma_\chi/(\overline{X}\sqrt{L})$, with σ_χ the standard deviation of the local spin susceptibility. This implies the correct evaluation of the thermodynamic limit even in the problematic $\xi \gg 1$ case. Incidentally, since σ_χ is smaller at higher temperatures and magnetic fields, this justifies the smaller error bars in these regions.

* fr.casola@gmail.com

- ¹ H. A. Bethe, Z. Phys. **71**, 205 (1931); P. W. Anderson, Mater. Res. Bull. **8**, 153 (1973).
- ² C. Dasgupta and S. K. Ma, Phys. Rev. B **22**, 1305 (1979).
- ³ D. S. Fisher, Phys. Rev. B **50**, 3799 (1994).
- ⁴ F. Iglói and C. Monthus, Phys. Rep. **412**, 277 (2005).
- ⁵ E. C. Andrade and M. Vojta, Eur. Phys. Lett. **97**, 37007 (2012).
- ⁶ Y.-C. Lin, R. Mélin, H. Rieger and F. Iglói, Phys. Rev. B **68**, 024424 (2003).
- ⁷ N. Laflorencie, D. Poilblanc, and M. Sigrist, Phys. Rev. B **71**, 212403 (2005).
- ⁸ A. Zheludev and T. Roscilde, arXiv:1305.1194 [cond-mat.str-el] (2013).
- ⁹ S. Ward, P. Bouillot, H. Ryll, K. Kiefer, K. W. Krämer, Ch. Rüegg, C. Kollath and T. Giamarchi, J. Phys.: Condens. Matter **25**, 014004 (2013).
- ¹⁰ G. Simutis, S. Gvasaliya, M. Månsson, A. L. Chernyshev, A. Mohan, S. Singh, C. Hess, A. T. Savici, A. I. Kolesnikov, A. Piovano, T. Perring, I. Zaliznyak, B. Büchner, A. Zheludev, accepted in Phys. Rev. Lett. **111** (2013).

- ¹¹ B. Bauer et al (ALPS collaboration), J. Stat. Mech. P05001 (2011).
- ¹² Y. Yamada, Z. Hiroi, and M. Takano, J. Solid State Chem. **156**, 101 (2001).
- ¹³ F. Casola, T. Shiroka, V. Glazkov, A. Feiguin, G. Dhalenne, A. Revcolevschi, A. Zheludev, H.-R. Ott, and J. Mesot, Phys. Rev. B **86**, 165111 (2012).
- ¹⁴ L. P. Kadanoff, Ann. Phys. **100**, 359 (1976).
- ¹⁵ T. Shiroka, F. Casola, V. Glazkov, A. Zheludev, K. Prša, H.-R. Ott, and J. Mesot, Phys. Rev. Lett. **106**, 137202 (2011).
- ¹⁶ M. Thede, F. Xiao, Ch. Baines, C. Landee, E. Morenzoni, and A. Zheludev, Phys. Rev. B **86**, 180407(R) (2012).
- ¹⁷ E. Yusuf and K. Yang, Phys. Rev. B **72**, 020403(R) (2005).
- ¹⁸ A. Zheludev, T. Masuda, G. Dhalenne, A. Revcolevschi, C. Frost, and T. Perring, Phys. Rev. B **75**, 054409 (2007).
- ¹⁹ J. C. Bonner and M. E. Fisher, Phys. Rev. **135**, A640 (1964).
- ²⁰ S. Bertaina and R. Hayn, Phys. Rev. B **73**, 212409 (2006).
- ²¹ T. Masuda, A. Zheludev, K. Uchinokura, J. H. Chung, and S. Park, Phys. Rev. Lett. **93**, 077206 (2004).

- ²² M. Kenzelmann, A. Zheludev, S. Raymond, E. Ressouche, T. Masuda, P. Böni, K. Kakurai, I. Tsukada, K. Uchinokura, and R. Coldea, *Phys. Rev. B* **64**, 054422 (2001).
- ²³ A. Joshi and Kun Yang, *Phys. Rev. B* **67**, 174403 (2003).
- ²⁴ R. J. Birgeneau, M. Greven, M. A. Kastner, Y. S. Lee, B. O. Wells, Y. Endoh, K. Yamada, and G. Shirane, *Phys. Rev. B* **59**, 13788 (1999).
- ²⁵ T. Masuda, A. Zheludev, K. Uchinokura, J. H. Chung, and S. Park, *Phys. Rev. Lett.* **96**, 169908 (2006).
- ²⁶ D. C. Johnston, R. K. Kremer, M. Troyer, X. Wang, A. Klümper, S. L. Bud'ko, A. F. Panchula, and P. C. Canfield, *Phys. Rev. B* **61**, 9558 (2000).
- ²⁷ I. Affleck, M. Oshikawa, *Phys. Rev. B* **60**, 1038 (1999).
- ²⁸ N. Shibata and K. Ueda, *J. Phys. Soc. Jpn.* **70**, 3690 (2001).
- ²⁹ E. Westerberg, A. Furusaki, M. Sigrist, and P. A. Lee, *Phys. Rev. Lett.* **75**, 4302 (1995).
- ³⁰ F. Alet, S. Wessel, and M. Troyer, *Phys. Rev. E* **71**, 036706 (2005).
- ³¹ W. G. Clark, M. E. Hanson, F. Lefloch, and P. Ségransan, *Rev. Sci. Instrum.* **66**, 2453 (1995).
- ³² R. K. Harris, E. D. Becker, S. M. Cabral de Menezes, R. Goodfellow, P. Grangers, *Pure Appl. Chem.* **73**, 1795 (2001).
- ³³ S. Miyahara, J.-B. Fouet, S. R. Manmana, R. M. Noack, H. Mayaffre, I. Sheikin, C. Berthier, and F. Mila, *Phys. Rev. B* **75** 184402 (2007).
- ³⁴ H. Shimazaki and S. Shinomoto, *Neural Comput.* **19**, 1503 (2007).
- ³⁵ H. Shimazaki and S. Shinomoto, *Neural Inf. Process. Syst.* **19**, 1289 (2007).
- ³⁶ A. Aharony and A. B. Harris, *Phys. Rev. Lett.* **77**, 3700 (1996).